



# Visible-Range Double Fano Resonance Metal–Insulator-Metal Plasmonic Waveguide for Optical Refractive Index Sensing

Shahab Tavana<sup>1</sup> · Shahram Bahadori-Haghighi<sup>1</sup>

Received: 10 July 2022 / Accepted: 26 October 2022 / Published online: 4 November 2022  
© The Author(s), under exclusive licence to Springer Science+Business Media, LLC, part of Springer Nature 2022

## Abstract

A metal–insulator-metal (MIM) structure consisting of a semi-circular resonant cavity (SCRC) and a circular split-ring resonator (SRR) is proposed and designed for optical sensing applications. The coupling between the SCRC and SRR can create dual Fano resonances in the visible range. The optical responses of the structure including transmittance spectra and magnetic field distributions are investigated using finite-difference time-domain (FDTD) method. According to the calculated transmittance spectra, the proposed optical sensor can support double Fano resonances as a result of the interaction between the narrow-band mode of SRR and broadband mode of SCRC. The light-matter interaction at the Fano resonance frequencies is highly enhanced so that a maximum sensitivity and figures of merit (FOM) of 579 nm/RIU and 12.46 are obtained, respectively. Our proposed design also exhibits a great linearity  $R^2$  value of 0.999987. For the sake of completeness, it is shown that the structure can result in an optical delay of about 0.05 ps corresponding to a group index of 14.6 that is potentially useful for plasmonic nanosensors and slow-light devices in the visible range of the spectrum.

**Keywords** Metal–insulator-metal waveguide · Dual Fano resonances · Visible sensor · Slow light · High linearity sensor · Refractive index sensor

## Introduction

In recent years, optical refractive index sensors have been widely used in biomedical, chemical, and food processing industries due to their advantages such as small size, high precision, and anti-interference [1–3]. The diffraction limit of traditional optics has severely restricted the development of modern optics to integrated optical devices. However, the proposal of surface plasmon polaritons (SPPs) can overcome the traditional optical diffraction limitation and confine light in subwavelength scales [4–6]. SPPs are types of collective oscillations which propagate along the interface of metal and insulator. In other words, the interaction of electromagnetic waves and free electrons at the interface of metal and insulator leads to a localized field and enhanced light confinement that is suitable for sensing applications [7–9]. Besides, the effect of SPPs on various

geometries including silver shells and silver films reveals that not only the electric field intensity on the surface of silver is enhanced but also the plasmon resonances can be adjusted [10, 11]. Among various waveguide devices based on SPPs, metal–insulator-metal (MIM) structures are of great interest due to their small mode size [12], strong confinement of light [13], short propagation length, and easy fabrication [14, 15]. MIM waveguides have already been designed and implemented for various applications [16, 17]. So far, many research studies have been reported on MIM-type SPP optical waveguides including filters [18, 19], all-optical switches [20, 21], demultiplexers [22], couplers [23], and Bragg’s reflectors [24]. In addition to MIM waveguides, there are some special resonance phenomena such as Fano resonance that can significantly increase light-matter interaction. Fano resonance occurs due to interference between a discrete state and a continuum band of states. In contrast to traditional Lorentz resonance, Fano resonance exhibits a sharp and asymmetric line shape that is very sensitive to structural parameters and surrounding medium environment [25, 26]. Fano resonance has potential applications in slow-light devices [27, 28], switches [29], and biosensors [30, 31]. MIM waveguides based on Fano resonances play critical

✉ Shahram Bahadori-Haghighi  
sbahadori@shirazu.ac.ir

<sup>1</sup> Department of Communications and Electronics, School of Electrical and Computer Engineering, Shiraz University, Shiraz, Iran

roles in refractive index sensors where the resonators are of different shapes such as rectangular [32], triangular [33], double ring [34], bowtie-shaped [35] and stub-shaped with defects [36].

Recently, various refractive index sensors based on MIM waveguides have been proposed. Some of them are based on traditional Lorentz resonances. For example, a multimode plasmonic sensor constructed by a square-ring-shaped with silver nanorods and a MIM waveguide was proposed in 2021. According to the presented results, the sensor exhibits high sensitivity, an acceptable figure of merit (FOM), and a quality factor (Q-factor) of about 2473 nm/RIU, 34.18 RIU<sup>-1</sup>, and 56.35, respectively [37]. Khani and Hayati [38] proposed another structure is made of an elliptical resonator, a silicon strip layer, and a MIM waveguide. The structure generates multiresonance modes in the transmittance spectrum where the FOM reached 282.5 RIU<sup>-1</sup> at the wavelength of 592 nm [38]. However, many researchers have already focused on the Fano resonances based on MIM waveguides due to their strong tunability in sensing devices. In 2020, a refractive index sensor was presented based on multiple Fano resonances in a MIM waveguide with a semi-circular cavity coupled to a cross-shaped cavity whereby one of the Fano resonances was located in the visible range. The sensitivity of the sensor was reported to be 525 nm/RIU and the FOM could reach 136 RIU<sup>-1</sup> [39]. A high Q-factor Fano resonance generated by a hybrid metamaterial waveguide was also presented in 2021 [40]. According to the results, an ultra-narrow Fano resonance linewidth of 1.7 nm and FOM of 236 in the visible wavelength range were achievable. Chao et al. [41] proposed an ultra-compact plasmonic waveguide, which offered multiple Fano resonance modes. It was shown that introducing an air path to a circular ring greatly influenced the effective coupling between the bus waveguides and the side-coupled resonator which enhanced the sensing performance and led to a refractive index and temperature sensitivity of 2900 nm/RIU and 1.13 nm/°C, respectively [41]. Another multiple Fano resonance mode for refractive index sensing applications was designed by Chau et al. [42] where they utilized dual air stubs, air path, and metal defects to improve light-matter interaction. The sensitivity of modes 1 and 2 are as high as 2600 nm/RIU and 1200 nm/RIU, respectively [42]. Wang et al. [43] also achieved independently adjustable triple Fano resonances by a square-ring cavity, an isosceles triangle cavity, and a bus waveguide. The obtained high sensitivity of 2259 nm/RIU could easily sense the plasma and glucose concentration [43]. A MIM waveguide structure with a resonator including three Ag baffles in a rectangular cavity was designed by Chou Chau et al. [44] where a high sensitivity of 3300 nm/RIU as well as a wide bandgap was obtained. It can be seen that

almost all of the structures operate in the infrared range, and, also, they have not considered the influence of the slow-light effect in their proposed structures.

In this paper, we propose a MIM plasmonic waveguide constructed by a semi-circular resonant cavity (SCRC) and a circular split-ring resonator (SRR) which can generate two distinct Fano resonances in the visible range for the first time. The transmittance and magnetic field distribution of the structure are calculated by using finite-difference time-domain (FDTD) method. After optimizing the geometrical parameters of the proposed structure, a sensitivity of as high as 579 nm/RIU is obtained. The results prove that the transmission and group index is suitable for producing the slow-light effect. Compared with other refractive index sensors of the same type, the proposed structure exhibits better simplicity, compactness, and sensitivity which provides a promising candidate for integrated optical sensing and biosensing in the visible range. According to the presented results, high linearity  $R^2$  values of more than 0.999987 are achieved for both Fano resonance peaks that are promising for sensing applications.

## Proposed Plasmonic Sensor

The three-dimensional (3D) schematic diagram of the proposed MIM plasmonic sensor composed of a SCRC coupled to a SRR is shown in Fig. 1a [45, 46]. The corresponding 2D model (the cross section at  $z=0$  in Fig. 1a) of the structure is also depicted in Fig. 1b where the geometrical parameters are indicated. As it can be seen, the SRR is created by introducing a split to a regular ring with a split angle of  $\theta$ . The orientation of SRR is measured by the angle  $\alpha$  between the center of the split and the x-axis. The parameter  $R$  denotes the outer radius of SRR and SCRC.  $g$  represents the gap between SRR and SCRC, and  $w$  is the width of the MIM waveguide. In the two-dimensional model, the blue and gray regions represent silver (Ag) and air with relative permittivity of  $\epsilon_m$  and  $\epsilon_i$ , respectively. In our proposed design, Ag is chosen due to its low power consumption and low absorption in contrast to gold and aluminum. Furthermore, from the practical point of view, Ag adheres well to the substrate and can be patterned easily with great etch selectivity using diluted nitric acid and water [47]. The proposed structure can be fabricated by the following steps: an Ag is deposited on a quartz substrate by chemical vapor deposition (CVD). Afterwards, the SCRC, the SRR, and the waveguide can be etched by the electron beam etching method [48, 49]. The frequency-dependent complex relative permittivity of Ag can be calculated using the Drude model [50, 51]:

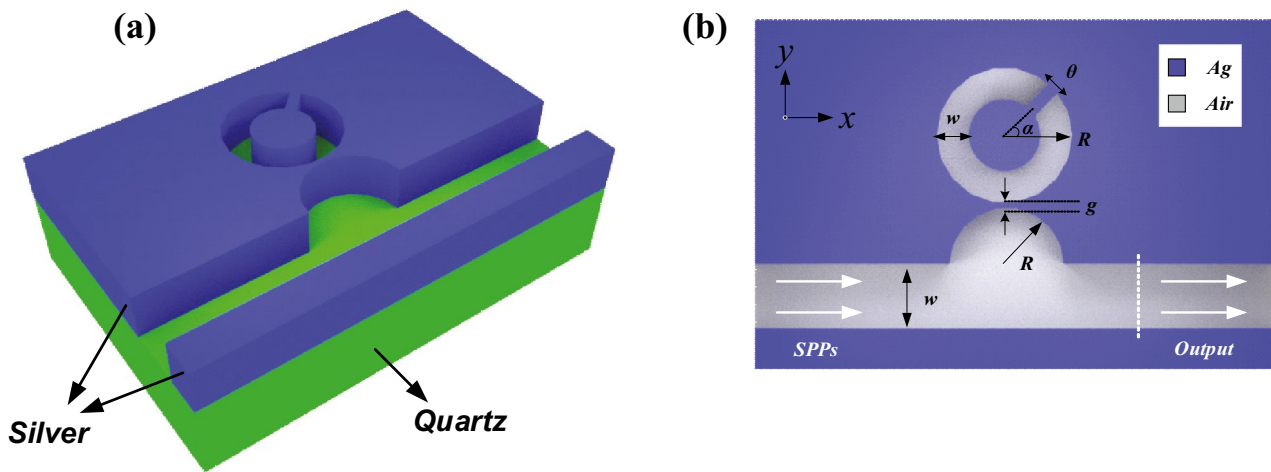


**Fig. 1** Schematic diagram of the proposed structure consisting of a MIM waveguide side-coupled to a SCRC and a SRR with outer radius  $R$  and split width corresponding to a sector angle  $\theta$ : **a** three-dimensional map; **b** 2D schematic of the structure

$$\epsilon_m(\omega) = \epsilon_\infty - \frac{\omega_p^2}{\omega(\omega + i\gamma)}, \tag{1}$$

where  $\epsilon_\infty = 3.7$  denotes the relative permittivity of Ag at an infinite frequency,  $\omega_p = 9.1$  eV refers to the plasma frequency of silver,  $\omega$  is the angular frequency of the incident light, and the electron collision frequency is  $\gamma = 0.018$  eV. When the incident light enters from the left port of the waveguide and propagates along the x-axis, it exits from the right port of the waveguide after coupling to the SRR. The transmittance of the structure is measured by two power monitors  $P_{out}$  and  $P_{in}$ , where they represent the output and input power. The transmittance spectra of the proposed MIM sensor are calculated by  $T = P_{out}/P_{in}$ . To investigate the transmittance, Ansys Lumerical 2020 software based on the FDTD method has been used where the computational cell is surrounded by perfectly matched layers (PMLs) and the maximum uniform mesh size is considered to be 0.5 nm. The widths of the MIM waveguide and SRR are fixed at  $w = 50$  nm so that only the fundamental transverse magnetic ( $TM_0$ ) mode is allowed to propagate through the MIM structure [52]. According to the standing wave theory, SRR can be regarded as a Fabry–Perot (F-P) resonator for which the resonant wavelengths can be obtained by the following relation [53–55]:

$$\lambda = \frac{2\text{Re}(n_{eff})L_{eff}}{m - \varphi/2\pi}, m = 1, 2, 3, \dots, \tag{2}$$

where  $n_{eff}$  is the waveguide effective mode index, and the effective Fabry–Perot cavity length of the SRR is  $L_{eff} = (1 - \theta/360^\circ)2\pi R_{eff}$  with  $R_{eff} = R - w/2$ . The parameter  $\varphi$  denotes the phase shift due to light reflection at either edge of the split in SRR, and  $m$  is the order of resonance mode.

### Simulations and Results

In order to investigate the transmittance spectrum of the MIM waveguide consisting of a SCRC coupled to a SRR, the geometric parameters are set as follows:  $w = 50$  nm,  $R = 90$  nm,  $g = 10$  nm,  $\theta = 10^\circ$ , and  $\alpha = 45^\circ$ . Figure 2 shows the transmittance spectra of the MIM waveguide with SCRC, SRR, and the entire structure. The blue curve represents the wide-band continuous state which is excited by the SCRC and the corresponding transmittance is approximately 0.4 that around which it fluctuates within a certain range. In order to create a narrow-band discrete state, the single SRR

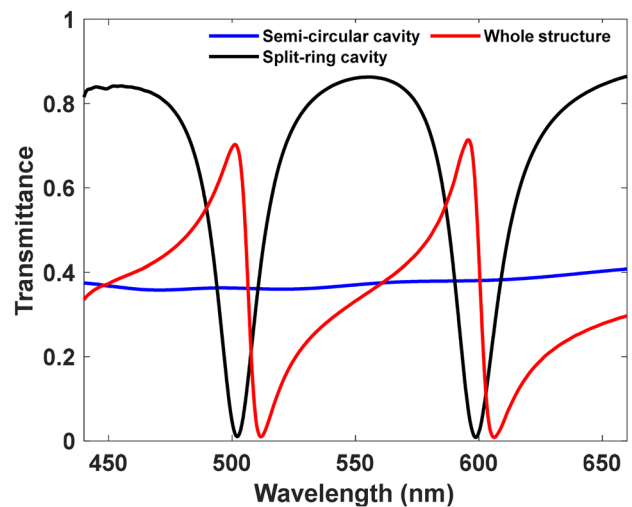


**Fig. 2** Transmittance spectra of the MIM waveguide with the SCRC (blue line), the SRR (black line), and the whole structure (red line)

is placed near the MIM waveguide that can generate two sharp stop bands at 502 nm and 598 nm. Therefore, the interference of the discrete states and the continuum state leads to the formation of double Fano resonances for the whole structure. These two Fano resonance peaks are named FR1 and FR2 that appear at the wavelengths of 501 nm and 596 nm, respectively. At these points, the transmittance attains the maximum value of 0.7.

The normalized magnetic field intensity distributions ( $H_z$ ) of the whole structure at  $\lambda = 501$  nm (FR1 peak) and 596 nm (FR2 peak) are depicted in Fig. 3a, b, respectively. The unit of the magnetic field is amperes per meter (A/m). The corresponding magnetic field profiles of the structure with the SRR at the two resonance peaks of 502 nm and 598 nm are also shown in Fig. 3c, d, respectively, which play the roles of discrete states in the Fano resonance mechanisms.

According to Fig. 3a, b, the proposed structure is asymmetric with respect to the  $y$ -axis, and the Fano resonance modes are divided into two parts by two nodes. Moreover, the two nodes are symmetric about the centerline of the split with the angle of  $\alpha = 45^\circ$  so that almost all the associated energy of FR1 or FR2 is concentrated within the split ring at the opposite sides of the nodes. As it is obviously seen, the magnetic fields in the SRR and SCRC are out of phase with each other so most of the input energy of SPPs is transmitted through the structure to the output port. However, when SCRC is removed from the structure, the supported modes will change. The number of nodes for even and odd modes are respectively determined by  $p = 2m$  and  $p = 2m' + 1$ . Therefore, the mode shown in Fig. 3c with three nodes is an odd mode while that illustrated in Fig. 3d with two nodes is an even mode. As it is shown in Fig. 3c, d, the magnetic

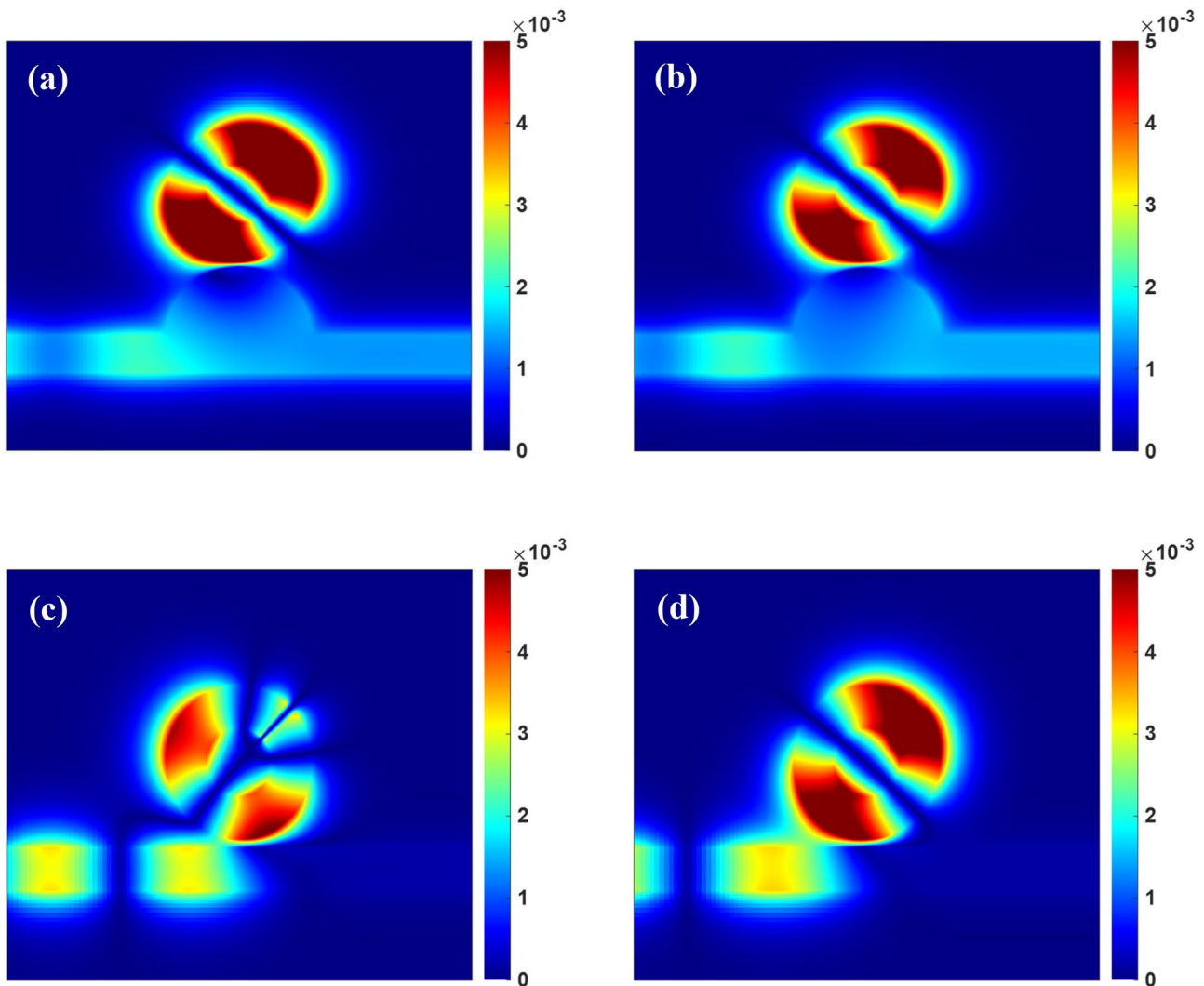


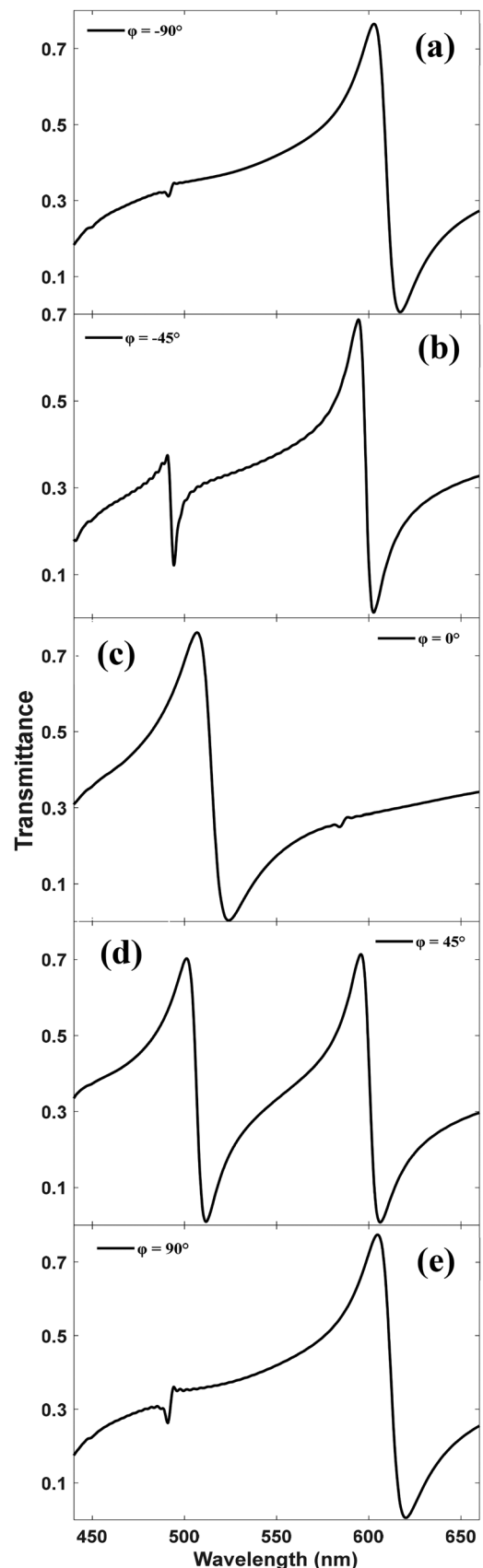
**Fig. 3** a–b Magnetic field patterns of FR1 and FR2 while c and d are the distributions of magnetic field intensity of the SRR coupled to the waveguide without the semi-circular cavity

**Fig. 4** Transmittance spectra of the proposed structure with different split angles

fields in the SRR and MIM waveguide are in phase with each other which results in a large amount of energy localized in the cavity.

The transmittance spectra of the structure for split angles ( $\alpha$ ) of  $\alpha = -90^\circ, -45^\circ, 0^\circ, 45^\circ,$  and  $90^\circ$  are calculated and shown in Fig. 4a–e. As it can be seen, the positions of resonance wavelengths are strongly affected by the split angle due to the coupling strength between the SCRC and SRR, and the effective refractive index  $n_{\text{eff}}$  will shift slightly. Furthermore, the transmittance of the two modes is independent of each other at different split angles, and the transmittance peaks of the two Fano resonances are altered by the split angle. The transmittance peaks of FR1 and FR2 are approximately the same for the cases of  $\alpha = -90^\circ$  and  $90^\circ$ . It is due to the fact that the structure is symmetric about the y-axis, while the structures in the cases of  $\alpha = 0^\circ, 45^\circ,$  and  $-45^\circ$  are all asymmetric about it. The weak FR1 and pronounced FR2 are obviously seen in Fig. 4a, e, which confirm the weaker coupling effect between SCRC and SRR at the FR1 mode. According to Fig. 4c, the optical response of the structure for  $\alpha = 0^\circ$  is totally different from the other cases so there is no obvious transmittance for FR2. Additionally, as shown in Fig. 4b, d, there exists a large difference between the FR1 transmittance amplitudes for  $\alpha = -45^\circ$  and  $45^\circ$ . It is obvious that two pronounced Fano resonances of FR1 and FR2 can be obtained for  $\alpha = 45^\circ$ . It is attributed to the strong confinement of SPPs and constructive interference between SRR and SCRC which enhances the resonance in the split ring. As seen in Fig. 4a–d, the difference between the transmittance peak and dip ( $\Delta D$ ) rises with the increase of  $\alpha$  in FR1 and the highest  $\Delta D$  takes place for two Fano resonances when  $\alpha = 45^\circ$  [56]. Hence, the proposed MIM structure with  $\alpha = 45^\circ$  is examined in the following.

Now, the effects of SCRC and SRR sizes on the aforementioned Fano resonances are investigated. The calculated transmittance spectra of the structures with different sector angles ( $\theta$ ) from  $0^\circ$  to  $10^\circ$  are depicted in Fig. 5a. In the case of  $\theta = 0^\circ$ , there is only one Fano resonance peak at  $\lambda = 605$  nm. Because there is no split in the ring and all the light is confined within the ring. When the sector angle starts to increase, two Fano resonances appear. As it can be seen in Fig. 5a, FR2 experiences an obvious redshift while there is a slight blueshift of FR1 when  $\theta$  increases from  $5^\circ$  to  $10^\circ$ . The variations of transmittance spectra for various outer radii ( $R$ ) of SRR and SCRC from 85 to 100 nm at the SRR width of 50 nm are calculated and plotted in Fig. 5b. The redshifts of the FR1 and FR2 take place by increasing  $R$  and the line shapes at the peaks become more and more asymmetrical which are obviously seen in Fig. 5b. Meanwhile, the transmittance of FR1 and FR2 decreases from 0.7





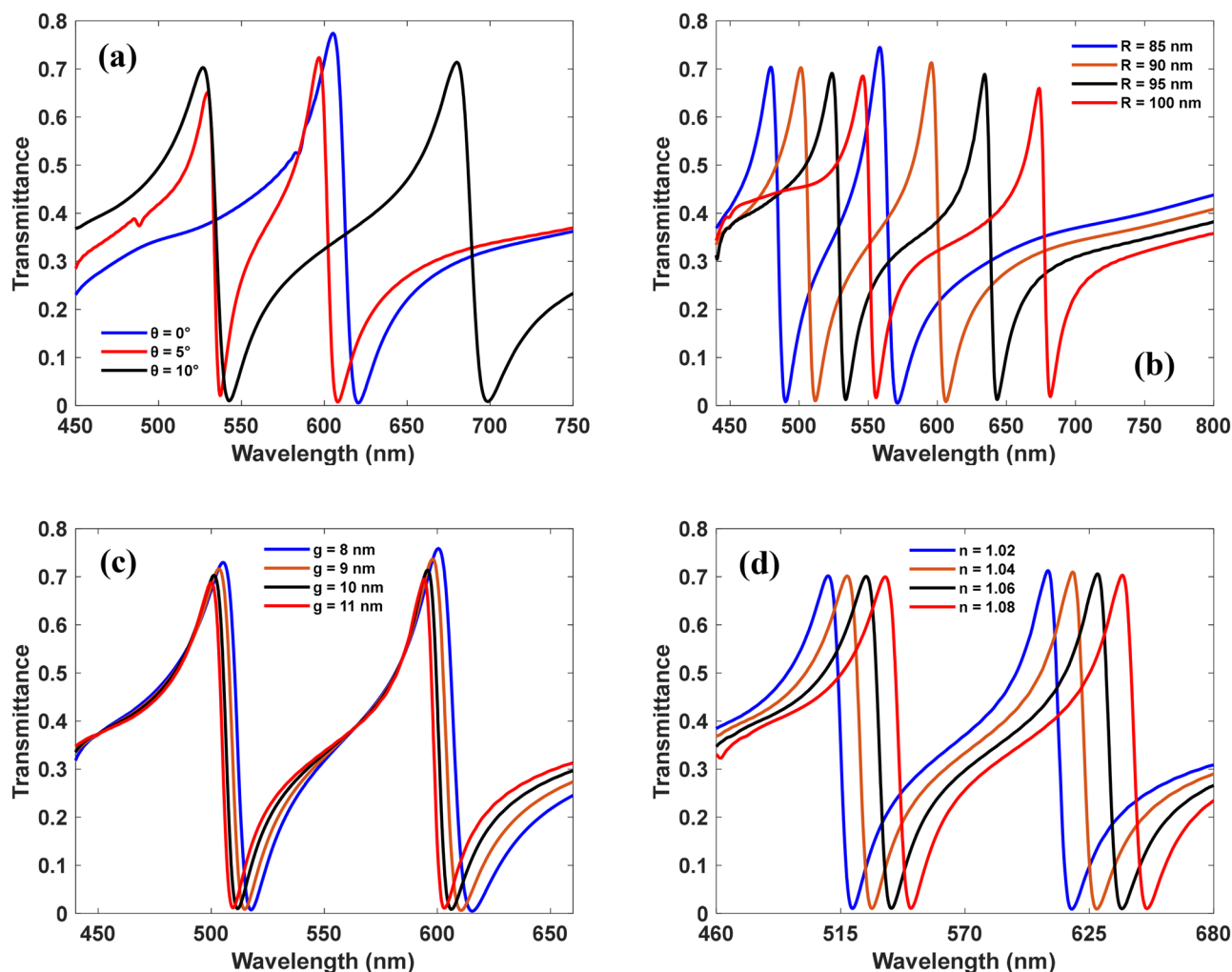


**Fig. 5** Transmittance spectra of the structures with **a** different split angles, **b** different outer radii of the SRR and SCRC, **c** different coupling distances, and **d** different analyte refractive indices

to 0.68 and 0.74 to 0.66, respectively. The gap size between the SRR and SCRC ( $g$ ) is another parameter that is investigated. The coupling distance  $g$  directly affects the coupling effect between the discrete state and the continuous state, which can optimize the location of two Fano resonances. The transmittance spectra of the proposed structure for  $g = 8, 9, 10,$  and  $11$  nm are shown in Fig. 5c. There are redshifts of FR1 and FR2 from 499 to 505 nm and 594 to 600 nm as the gap size changes from 11 to 8 nm, respectively. In addition, the corresponding amplitudes of the Fano resonances increase as  $g$  starts to reduce from 11 to 8 nm. It should be mentioned that the SRR and SCRC in the proposed structure can be filled by the desired analyte so that its corresponding refractive index changes the resonance wavelengths.

In order to investigate the sensing characteristics of the proposed structure, the analyte refractive index within the SRR and SCRC is considered to be changed from 1.02 to

1.08. The transmittance spectra of the structure for different analyte refractive indices are shown in Fig. 5d. It is clear that the transmittance peaks shift to the higher wavelengths by increasing the refractive index while the peak amplitudes remain approximately constant. As a result, the maximum sensitivities ( $\Delta\lambda/\Delta n$ ) at the two Fano resonances of FR1 and FR2 are respectively as high as 433 nm/RIU and 579 nm/RIU. Another key factor to describe the sensing performance is FOM which is defined as  $FOM = \Delta T / (T \cdot \Delta n)$ , where  $T$  is the transmission of the structure and  $\Delta T$  is the relative transmission variation that is induced by the refractive index  $\Delta n$  at the fixed wavelength. According to the calculations, the FOM at the two resonances of FR1 and FR2 are also calculated to be 8 and 12.46, respectively. In Table 1, the sensitivity of the proposed structure is compared with the previously reported papers at the visible range. As it can be seen, our achieved sensitivity is higher than most of the reported

**Table 1** Comparison of the sensitivity with the previously reported references in the visible range

Source	Number of Fano resonances	Sensitivity (nm/RIU)
[39]	1	525
[59]	1	550
[25]	1	596
[60]	1	530
[40]	1	196
<b>This work</b>	2	579

sensitivities in the visible range. The resonance wavelengths of FR1 and FR2 as functions of analyte refractive index are plotted in Fig. 6a where they are also fitted with straight lines of indicated linear equations. According to Fig. 6a, the

linearity  $R^2$  values of the FR1 and FR2 are calculated to be as high as 0.99996 and 0.999987, respectively.

For the sake of completeness, it can be shown that the proposed structure supports the slow-light effect and the geometrical parameters are as follows:  $w = 50 \text{ nm}$ ,  $R = 90 \text{ nm}$ ,  $g = 10 \text{ nm}$ ,  $\theta = 10^\circ$ , and  $\alpha = 45^\circ$ , and  $L = 0.9 \text{ }\mu\text{m}$ . Group index  $n_g$  as the criterion of the slow-light effect is expressed as [57, 58]:

$$n_g = \frac{c}{v_g} = \frac{c}{L} \tau_g = \frac{c}{L} \cdot \frac{d\psi(\omega)}{d\omega} \tag{3}$$

where  $c$  denotes the speed of light in vacuum,  $L$  is the distance between the light source and the detector,  $v_g$  represents the group velocity, and  $\tau_g$  is the delay time; the phase response of the designed structure is shown in Fig. 6b where a large phase shift around the resonance wavelengths

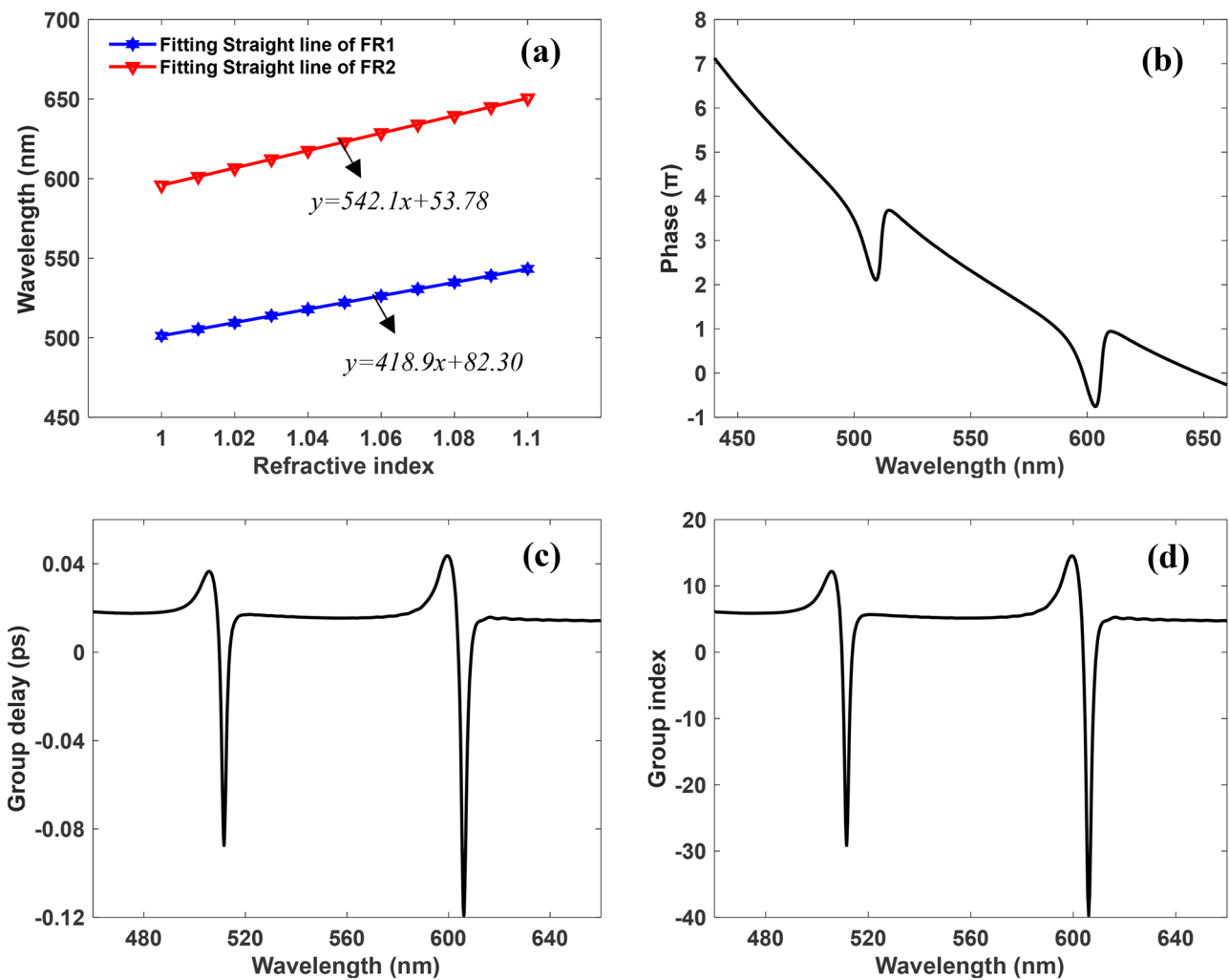


**Fig. 6** a Variations of Fano resonance wavelengths as functions of analyte refractive index. b The phase shift, c group delay, and d group index of the proposed structure

of 509 nm and 603 nm is depicted. The positive slopes of phase response occur at the dips of the resonances due to the abnormal dispersion while the negative slopes because of normal dispersion occur at the peaks. Such negative slopes result in enhanced group delays up to 0.04 ps and 0.05 ps at the two Fano resonances as shown in Fig. 6c. Correspondingly, according to Fig. 6d, the group indices of FR1 and FR2 reach 12.2 and 14.6, respectively.

## Conclusion

In this work, a MIM structure with a SCRC and a SRR is proposed for optical biosensing. The structure is analyzed by the FDTD method. According to the simulation results, double Fano resonances are excited in the visible range of the electromagnetic spectrum. It is illustrated that the positions of the two Fano resonances strongly depend on structural parameters such as the radii of SRR and SCRC, coupling distance, sector angle, and size of the split. The maximum sensitivity of refractive index sensing can reach 579 nm/RIU, with a maximum FOM of 12.46. Meanwhile, the structure exhibits an extremely high linearity  $R^2$  value of 0.999987 that is really promising for sensing applications. In addition, maximum optical delay and group index of about 0.05 ps and 14.6 are respectively obtained which confirm the slow-light effect in our proposed structure.

**Author Contribution** Both authors worked on the study conception and design. Simulations were carried out by Shahab Tavana. Also, the first draft of the manuscript was written by Shahab Tavana, and then it was edited by Dr. Shahram Bahadori-Haghighi.

**Data Availability** All data generated or analyzed during this study are included in this article.

## Declarations

**Consent to Participate** Informed consent was obtained from all participants.

**Consent for Publication** Informed consent for publication was obtained from all authors.

**Conflict of Interest** The authors declare no competing interests.

## References

- Danaie M, Kiani B (2018) Design of a label-free photonic crystal refractive index sensor for biomedical applications. *Photonics Nanostruct Fundam Appl* 31:89–98
- Xu Y, Bai P, Zhou X, Akimov Y, Png CE, Ang LK et al (2019) Optical refractive index sensors with plasmonic and photonic structures: promising and inconvenient truth. *Adv Opt Mater* 7(9):1801433
- Schuller JA, Barnard ES, Cai W, Jun YC, White JS, Brongersma ML (2010) Plasmonics for extreme light concentration and manipulation. *Nat Mater* 9(3):193–204
- Moreira R, Wolfe J, Taylor SD (2021) A high-yielding solid-phase total synthesis of daptomycin using a Fmoc SPPS stable kynurenine synthon. *Org Biomol Chem* 19(14):3144–3153
- Qiao L, Zhang G, Wang Z, Fan G, Yan Y (2019) Study on the Fano resonance of coupling M-type cavity based on surface plasmon polaritons. *Opt Commun* 433:144–149
- Kazanskiy N, Khonina S, Butt M (2020) Plasmonic sensors based on metal-insulator-metal waveguides for refractive index sensing applications: a brief review. *Physica E* 117:113798
- Fan JA, Wu C, Bao K, Bao J, Bardhan R, Halas NJ et al (2010) Self-assembled plasmonic nanoparticle clusters. *Science* 328(5982):1135–1138
- Yu S, Su Y, Sun Z, Zhao T, Yu J (2021) Multi-Fano resonances in MIM waveguides coupled with split annular cavity connected with rectangular resonator and application for multichannel refractive index sensor. *J Nanophotonics* 15(1):016004
- Refrakti S, Hayashi S, Ishitobi H, Nesterenko DV, Rahmouni A, Inouye Y et al (2018) Resolution enhancement of plasmonic sensors by metal-insulator-metal structures. *Ann Phys* 530(4):1700411
- Chau Y-F, Yeh H-H, Tsai D (2010) Surface plasmon resonances effects on different patterns of solid-silver and silver-shell nanocylindrical pairs. *J Electromagn Waves Appl* 24(8–9):1005–1014
- Hsieh L-Z, Chau Y-FC, Lim CM, Lin M-H, Huang HJ, Lin C-T et al (2016) Metal nano-particles sizing by thermal annealing for the enhancement of surface plasmon effects in thin-film solar cells application. *Opt Commun* 370:85–90
- Moon K, Lee T-W, Lee YJ, Kwon S-H (2017) A metal-insulator-metal deep subwavelength cavity based on cutoff frequency modulation. *Appl Sci* 7(1):86
- Zegaar I, Hocini A (2021) Modeling and analysis of the RI sensitivity of plasmonic sensor based on MIM waveguide-coupled structure. In *J Phys Conf Ser* (Vol. 1859, No. 1, pp. 012024): IOP Publishing
- Singh L, Iadicicco A, Agrawal N, Saha C, Chauhan R (2022) A compact formulation of all optical signal router by using plasmonic waveguides. *Opt Quant Electron* 54(8):1–10
- Khani S, Hayati M (2022) Optical sensing in single-mode filters base on surface plasmon H-shaped cavities. *Opt Commun* 505:127534
- Fang Y, Sun M (2015) Nanoplasmonic waveguides: towards applications in integrated nanophotonic circuits. *Light Sci Appl* 4(6):e294–e294
- Lu Q, Chen D, Wu G (2013) Low-loss hybrid plasmonic waveguide based on metal ridge and semiconductor nanowire. *Opt Commun* 289:64–68
- Chau Y-FC, Chao C-TC, Chiang H-P (2020) Ultra-broad bandgap metal-insulator-metal waveguide filter with symmetrical stubs and defects. *Results Phys* 17:103116
- Neutens P, Lagae L, Borghs G, Van Dorpe P (2012) Plasmon filters and resonators in metal-insulator-metal waveguides. *Opt Express* 20(4):3408–3423
- Khani S, Danaie M, Rezaei P (2020) Hybrid all-optical infrared metal-insulator-metal plasmonic switch incorporating photonic crystal bandgap structures. *Photonics Nanostruct Fundam Appl* 40:100802
- Khani S, Danaie M, Rezaei P (2021) Plasmonic all-optical metal-insulator-metal switches based on silver nano-rods, comprehensive theoretical analysis and design guidelines. *J Comput Electron* 20(1):442–457
- Ghasemi MR, Bayati MS (2021) Proposal for metal-insulator-metal plasmonic power splitter and demultiplexer suitable for implementation in optical switches. *IET Optoelectron* 15:200–206
- Stoja E, Frezza F (2013) Metal-insulator-metal (mim) plasmonic waveguide based directional couplers operating at telecom



- wavelengths. In 2013 6th UK, Europe, China Millimeter Waves and THz Technology Workshop (UCMMT) (pp. 1–2): IEEE
24. Zeng L, Li J, Cao C, Li X, Zeng X, Yu Q et al (2022) An integrated-plasmonic chip of Bragg reflection and Mach-Zehnder interference based on metal-insulator-metal waveguide. *Photonic Sens* 12(3):1–10
  25. Zhang Z, Luo L, Xue C, Zhang W, Yan S (2016) Fano resonance based on metal-insulator-metal waveguide-coupled double rectangular cavities for plasmonic nanosensors. *Sensors* 16(5):642
  26. Limonov MF, Rybin MV, Poddubny AN, Kivshar YS (2017) Fano resonances in photonics. *Nat Photonics* 11(9):543–554
  27. Chen H-J (2020) Fano resonance induced fast to slow light in a hybrid semiconductor quantum dot and metal nanoparticle system. *Laser Phys Lett* 17(2):025201
  28. Chen H-J (2020) Majorana fermions induced Fano resonance and fast-to-slow light in a hybrid semiconductor/superconductor ring device. *Quantum Inf Process* 19(6):1–19
  29. Zhou YJ, Dai LH, Li QY, Xiao ZY (2020) Two-way Fano resonance switch in plasmonic metamaterials. *Front Phys* 483
  30. Parizi MS, Saleemizadehparizi F, Zarasvand MM, Abdolhosseini S, Bahadori-Haghighi S, Khalilian A (2021) High-performance graphene-based biosensor using a metasurface of asymmetric silicon disks. *IEEE Sensors J*
  31. Khonina S, Kazanskiy N, Butt M, Kaźmierczak A, Piramidowicz R (2021) Plasmonic sensor based on metal-insulator-metal waveguide square ring cavity filled with functional material for the detection of CO<sub>2</sub> gas. *Opt Express* 29(11):16584–16594
  32. Chao C-TC, Chau Y-FC, Mahadi AH, Kooh MRR, Kumara N, Chiang H-P (2021) Plasmonic refractive index sensor based on the combination of rectangular and circular resonators including baffles. *Chin J Phys* 71:286–299
  33. Wang S, Yu S, Zhao T, Wang Y, Shi X (2020) A nanosensor with ultra-high FOM based on tunable malleable multiple Fano resonances in a waveguide coupled isosceles triangular resonator. *Opt Commun* 465:125614
  34. Shao Z, Yan S, Wen F, Wu X, Hua E (2021) Double ring nanostructure with an internal cavity and a multiple Fano resonances system for refractive index sensing. *Appl Opt* 60(22):6623–6631
  35. Chou Chau Y-F (2021) Multiple-mode bowtie cavities for refractive index and glucose sensors working in visible and near-infrared wavelength ranges. *Plasmonics* 16(5):1633–1644
  36. Chau Y-FC (2020) Mid-infrared sensing properties of a plasmonic metal-insulator-metal waveguide with a single stub including defects. *J Phys D Appl Phys* 53(11):115401
  37. Chou Chau Y-F, Ming TY, Chou Chao C-T, Thotagamuge R, Kooh MRR, Huang HJ et al (2021) Significantly enhanced coupling effect and gap plasmon resonance in a MIM-cavity based sensing structure. *Sci Rep* 11(1):1–17
  38. Khani S, Hayati M (2021) An ultra-high sensitive plasmonic refractive index sensor using an elliptical resonator and MIM waveguide. *Superlattices Microstruct* 156:106970
  39. Qi Y-P, Wang L-Y, Zhang Y, Zhang T, Zhang B-H, Deng X-Y et al (2020) Multiple Fano resonances in metal-insulator-metal waveguide with umbrella resonator coupled with metal baffle for refractive index sensing. *Chin Phys B* 29(6):067303
  40. Yang H, Chen Y, Liu M, Xiao G, Luo Y, Liu H et al (2021) High Q-factor hybrid metamaterial waveguide multi-Fano resonance sensor in the visible wavelength range. *Nanomaterials* 11(6):1583
  41. Chao C-TC, Chau Y-FC, Chiang H-P (2021) Multiple Fano resonance modes in an ultra-compact plasmonic waveguide-cavity system for sensing applications. *Results Phys* 27:104527
  42. Chau Y-FC, Chou Chao C-T, Jumat SZBH, Kooh MRR, Thotagamuge R, Lim CM et al (2021) Improved refractive index-sensing performance of multimode Fano-resonance-based metal-insulator-metal nanostructures. *Nanomaterials* 11(8):2097
  43. Wang M, Tian H, Liu X, Li J, Liu Y (2022) Multiparameter sensing based on tunable Fano resonances in MIM waveguide structure with square-ring and triangular cavities. In *Photonics* (Vol. 9, No. 5, pp. 291): MDPI
  44. Chou Chau Y-F, Chou Chao C-T, Huang HJ, Kooh MRR, Kumara NTRN, Lim CM et al (2020) Ultrawide bandgap and high sensitivity of a plasmonic metal-insulator-metal waveguide filter with cavity and baffles. *Nanomaterials* 10(10):2030
  45. Chao C-TC, Chau Y-FC, Chiang H-P (2021) Highly sensitive metal-insulator-metal plasmonic refractive index sensor with a centrally coupled nanoring containing defects. *J Phys D Appl Phys* 54(11):115301
  46. Chau Y-FC, Chao CTC, Huang HJ, Wang Y-C, Chiang H-P, Idris MNSIM et al (2019) Strong and tunable plasmonic field coupling and enhancement generating from the protruded metal nanorods and dielectric cores. *Results Phys* 13:102290
  47. Yang R, Lu Z (2012) Subwavelength plasmonic waveguides and plasmonic materials. *Int J Opt* 2012
  48. Cong W, Fang Z, Nam-Young K (2010) Development and characterization of metal-insulator-metal capacitors with SiN<sub>x</sub> thin films by plasma-enhanced chemical vapor deposition. *Chin Phys Lett* 27(7):078101
  49. Zhu J, Lou J (2020) High-sensitivity Fano resonance temperature sensor in MIM waveguides coupled with a polydimethylsiloxane-sealed semi-square ring resonator. *Results Phys* 18:103183
  50. Zhu J, Li N (2020) MIM waveguide structure consisting of a semi-circular resonant cavity coupled with a key-shaped resonant cavity. *Opt Express* 28(14):19978–19987
  51. Butt M, Khonina S, Kazanskiy N (2019) Plasmonic refractive index sensor based on metal-insulator-metal waveguides with high sensitivity. *J Mod Opt* 66(9):1038–1043
  52. Fang Y, Wen K, Qin Y, Li Z, Wu B (2019) Multiple fano resonances in an end-coupled MIM waveguide system. *Opt Commun* 452:12–17
  53. Chen J, Li J, Liu X, Rohimah S, Tian H, Qi D (2021) Fano resonance in a MIM waveguide with double symmetric rectangular stubs and its sensing characteristics. *Opt Commun* 482:126563
  54. Li Z, Wen K, Chen L, Lei L, Zhou J, Zhou D et al (2019) Refractive index sensor based on multiple Fano resonances in a plasmonic MIM structure. *Appl Opt* 58(18):4878–4883
  55. Tan YM, Chao C-TC, Kooh MRR, Huang HJ, Thotagamuge R, Lim CM et al (2022) Mid infrared sensing structure based on a metal-insulator-metal waveguides with a triangular-shaped resonator. *Opt Commun* 516:128282
  56. Chou Chao C-T, Chou Chau Y-F, Chiang H-P (2022) Breaking the symmetry of a metal-insulator-metal-based resonator for sensing applications. *Nanoscale Res Lett* 17(1):1–14
  57. Akhavan A, Ghafoorifard H, Abdolhosseini S, Habibiyan H (2017) Plasmon-induced transparency based on a triangle cavity coupled with an ellipse-ring resonator. *Appl Opt* 56(34):9556–9563
  58. Xie Y, Chai J, Ye Y, Song T, Liu B, Zhang L et al (2021) A tunable slow light device with multiple channels based on plasmon-induced transparency. *Plasmonics* 16(5):1809–1816
  59. Yang Q, Liu X, Guo F, Bai H, Zhang B, Li X et al (2020) Multiple Fano resonance in MIM waveguide system with cross-shaped cavity. *Optik* 220:165163
  60. Chen Z-Q, Qi J-W, Chen J, Li Y-D, Hao Z-Q, Lu W-Q et al (2013) Fano resonance based on multimode interference in symmetric plasmonic structures and its applications in plasmonic nanosensors. *Chin Phys Lett* 30(5):057301

**Publisher's Note** Springer Nature remains neutral with regard to jurisdictional claims in published maps and institutional affiliations.

Springer Nature or its licensor (e.g. a society or other partner) holds exclusive rights to this article under a publishing agreement with the author(s) or other rightsholder(s); author self-archiving of the accepted manuscript version of this article is solely governed by the terms of such publishing agreement and applicable law.